Structure of human Mad1 C-terminal domain reveals its involvement in kinetochore targeting

Soonjoung Kim[a,b,1], Hongbin Sun[a,1,2], Diana R. Tomchick[c], Hongtao Yu[a,b,3], and Xuelian Luo[a,3]

[a]Department of Pharmacology, [b]Howard Hughes Medical Institute, and [c]Department of Biochemistry, University of Texas Southwestern Medical Center, 6001 Forest Park Road, Dallas, TX 75390

Edited by Edward D. Salmon, University of North Carolina, Chapel Hill, NC, and accepted by the Editorial Board February 28, 2012 (received for review November 4, 2011)

The spindle checkpoint prevents aneuploidy by delaying anaphase onset until all sister chromatids achieve proper microtubule attachment. The kinetochore-bound checkpoint protein complex Mad1-Mad2 promotes the conformational activation of Mad2 and serves as a catalytic engine of checkpoint signaling. How Mad1 is targeted to kinetochores is not understood. Here, we report the crystal structure of the conserved C-terminal domain (CTD) of human Mad1. Mad1 CTD forms a homodimer and, unexpectedly, has a fold similar to those of the kinetochore-binding domains of Spc25 and Csm1. Nonoverlapping Mad1 fragments retain detectable kinetochore targeting. Deletion of the CTD diminishes, does not abolish, Mad1 kinetochore localization. Mutagenesis studies further map the functional interface of Mad1 CTD in kinetochore targeting and implicate Bub1 as its receptor. Our results indicate that CTD is a part of an extensive kinetochore-binding interface of Mad1, and rationalize graded kinetochore targeting of Mad1 during checkpoint signaling.

dimerization | mitosis | X-ray crystallography | multivalency | chromosome

Aneuploidy is a major form of genomic instability in human cancers and can result from chromosome missegregation in mitosis. The spindle checkpoint is a cell-cycle surveillance system that guards against chromosome missegregation (1–3). Unattached kinetochores that exist intrinsically during normal prometaphase or as a consequence of spindle damage caused by exogenous chemical agents activate the checkpoint. The spindle checkpoint proteins, including Bub1, BubR1, Bub3, Mps1, Mad1, and Mad2, are recruited to unattached kinetochores in a hierarchical fashion and undergo enzymatic and conformational activation. The activated checkpoint proteins collaborate to inhibit APC/C^{Cdc20} (the anaphase-promoting complex/cyclosome bound to its mitotic activator Cdc20) (4–6), thereby stabilizing the APC/C substrates, securin and cyclin B1, and delaying anaphase onset until all kinetochores reach proper spindle attachment.

The constitutive Mad1-Mad2 core complex is a downstream component of the kinetochore-targeting hierarchy. The recruitment of Mad1-Mad2 to unattached kinetochores requires upstream kinetochore-bound components, including the Ndc80 complex consisting of Ndc80, Nuf2, Spc25, and Spc24 (7, 8). At the kinetochores, the Mad1-Mad2 core complex catalyzes the conformational activation of the unusual two-state protein Mad2, which has two natively folded conformers, open-Mad2 (O-Mad2 or N1-Mad2) and closed-Mad2 (C-Mad2 or N2-Mad2) (9–16). C-Mad2 in the Mad1-Mad2 core complex recruits cytosolic O-Mad2 through asymmetric dimerization and converts O-Mad2 into intermediate Mad2 (I-Mad2) or unliganded C-Mad2, which then binds to Cdc20. Formation of the Mad2-Cdc20 complex further promotes the binding of BubR1-Bub3 to Cdc20, forming the APC/C-inhibitory mitotic checkpoint complex (17). Thus, the Mad1-Mad2 core complex is a key catalytic engine of the spindle checkpoint.

Despite the importance of kinetochore-bound Mad1 in the spindle checkpoint, the mechanism of its kinetochore targeting is not understood. A C-terminal fragment of yeast Mad1 containing the highly conserved C-terminal domain (CTD) is necessary and sufficient for its kinetochore localization and checkpoint function (18). By contrast, an N-terminal fragment of *Xenopus* Mad1 lacking the CTD has been shown to localize to kinetochores (19). Finally, mutation of T680, a residue within the CTD and a potential Plk1 phosphorylation site, in human Mad1 has been reported to diminish its kinetochore localization (20). It is thus unclear whether Mad1 has conserved kinetochore-targeting domains. The kinetochore receptor or receptors of Mad1 are also unknown.

In this study, we have determined the crystal structure of the CTD of human Mad1. Unexpectedly, Mad1 CTD has a fold similar to those of the kinetochore-targeting domains of the Ndc80 complex component Spc25 and the yeast monopolin subunit Csm1, despite the lack of obvious sequence similarity. We show that nonoverlapping fragments of Mad1 can achieve detectable kinetochore targeting. Deletion of Mad1 CTD diminishes, does not abolish, Mad1 kinetochore targeting. Structure-based mutagenesis identifies a conserved RLK motif in Mad1 CTD critical for Mad1 kinetochore targeting in human cells. Interestingly, the same RLK motif is required for the checkpoint-stimulated Mad1-Bub1 interaction in yeast (21). Consistently, Bub1 is required for Mad1 kinetochore targeting in human cells, and depletion of Bub1 by RNA interference (RNAi) does not further reduce the kinetochore targeting of a Mad1 RLK-motif mutant. These results implicate Bub1 as a possible kinetochore receptor for Mad1 CTD. Therefore, Mad1 has an unusually extensive kinetochore-binding interface with multiple quasi-independent contacting sites, one of which involves the CTD.

Results

Mad1 CTD Forms a Dimer and Has a Fold Similar to Spc25. Mad1 contains an N-terminal coiled coil domain and a CTD (Fig. 1*A*). The Mad2-interacting motif (MIM) is located just N-terminal to the CTD. The structure of a 120-residue Mad2-binding fragment of human Mad1 bound to Mad2 had been previously determined (11). Other domains of Mad1 had not been structurally characterized. Because Mad1 CTD was highly conserved from yeast to man, we sought to determine its structure. We expressed and purified a series of CTD-containing human Mad1 fragments with different N-terminal boundaries and examined them using nuclear magnetic resonance (NMR) spectroscopy. Heteronuclear single

Author contributions: H.Y. and X.L. designed research; S.K., H.S., and X.L. performed research; S.K., D.R.T., H.Y., and X.L. analyzed data; and H.Y. and X.L. wrote the paper.

The authors declare no conflict of interest.

This article is a PNAS Direct Submission. E.D.S. is a guest editor invited by the Editorial Board.

Data deposition: The atomic coordinates have been deposited in the Protein Data Bank, www.pdb.org (PDB code 4DZO).

[1]S.K. and H.S. contributed equally to this work.

[2]Present address: Bio-NMR lab, High Magnetic Field Laboratory, Chinese Academy of Sciences, Hefei Institutes of Physical Sciences, Hefei, Anhui 230031, China.

[3]To whom correspondence may be addressed. E-mail: hongtao.yu@utsouthwestern.edu or xuelian.luo@utsouthwestern.edu.

This article contains supporting information online at www.pnas.org/lookup/suppl/doi:10.1073/pnas.1118210109/-/DCSupplemental.

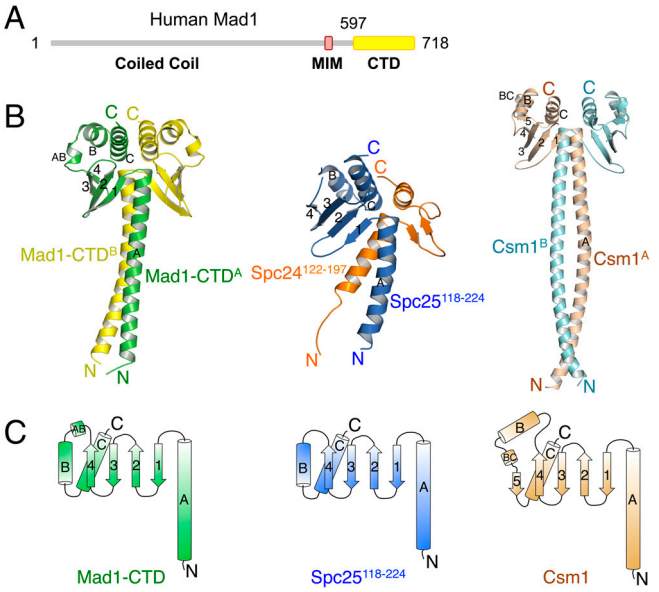

Fig. 1. Structure of the Mad1 CTD reveals fold similarity to the Ndc80 complex subunit Spc25 and the monopolin subunit Csm1. (*A*) Domain architecture of human Mad1. MIM, Mad2-interacting motif. CTD, C-terminal domain. (*B*) Ribbon diagrams of human Mad1 CTD homodimer (left), the Spc25-Spc24 CTD heterodimer (center; PDB code: 2VE7), and the Csm1 homodimer (right; PDB code: 3N4X). (*C*) Topology diagrams of Mad1 CTD (left), Spc25 CTD (middle), and Csm1 (right). All ribbon diagrams were generated using the program Pymol (http://www.pymol.org).

quantum correlation spectra revealed that the Mad1 CTD fragment containing residues 597–718 was well folded and had no flexible regions (Fig. S1*A*). Based on gel filtration chromatography, it had a native molecular mass of about 35 kDa, consistent with it being a homodimer (Fig. S1*B*). We next obtained crystals of selenium-methionine-labeled Mad1 CTD that diffracted to 1.75 Å and determined the structure of Mad1 CTD by the single wavelength anomalous dispersion (SAD) method (Table S1).

Mad1 CTD is indeed a homodimer and contains a coiled-coil stem and a globular head (Fig. 1*B*). Each monomer folds into a long helix (αA), a four-stranded antiparallel β sheet, a short helix (αAB), and 2 C-terminal helices (αB and αC) (Fig. 1 *B* and *C*). The N-terminal segments of two αA helices (one from each monomer) form the stem. αC and the C-terminal end of αA mediate the dimerization of the globular head. The fold of Mad1 CTD was strikingly similar to those of the kinetochore-targeting C-terminal domains of Spc25 (a subunit of the microtubule-binding Ndc80 kinetochore complex) and Csm1 (a subunit of the yeast monopolin complex) (Fig. 1 *B* and *C*) (22–24). This fold was also related to those of the RWD (RING finger-, WD-repeat-, and DEAD-like proteins) domain and ubiquitin-conjugating enzymes (25, 26). The fold similarity between Mad1 CTD and the CTDs of Spc25 and Csm1 was unexpected, as they share no obvious sequence similarity. Both CTDs of Mad1 and Csm1 form homodimers while Spc25 forms a heterodimer with the CTD of another Ndc80 subunit Spc24. Spc24 CTD is topologically related, but not identical, to Spc25 CTD (22, 23). The Mad1 CTD homodimer is thus structurally similar to the Spc25-Spc24 CTD heterodimer and to the Csm1 homodimer (Fig. 1*B*).

Mad1 Has Multiple Quasi-Independent Kinetochore-Binding Interfaces. The globular CTD heterodimer of Spc25 and Spc24 mediates the kinetochore targeting of the Ndc80 complex through interactions with the Mis12 complex (23, 27). Similarly, the globular CTD homodimer of Csm1 has also been shown to bind to kinetochores and interact with both the Mis12 complex and CENP-C (centromere protein C) (24). The unexpected structural similarity between Mad1 CTD and well established kinetochore-targeting domains prompted us to test whether the CTD was indeed involved in kinetochore targeting of human Mad1. On the other hand, previous studies had shown that the N-terminal domain of *Xenopus* Mad1 was critical for kinetochore targeting (19). To systematically define the kinetochore-binding domains of human Mad1, we created truncation mutants of Myc-Mad1-5A and examined their kinetochore localization using immunofluorescence (Fig. 2). Overexpression of Mad1 caused spindle checkpoint defects by titrating free Mad2 (Fig. S2 *A* and *B*) (19), hindering our detection of ectopically expressed Mad1 protein at kinetochores. We thus created a Mad1-5A mutant with the MIM mutated to alanines. Myc-Mad1-5A no longer had detectable binding to Mad2, even though it formed mixed dimers with the endogenous Mad1 (Fig. S2*C*). Overexpression of Myc-Mad1-5A did not cause strong spindle checkpoint defects. The Mad1 deletion mutants were thus constructed from Myc-Mad1-5A.

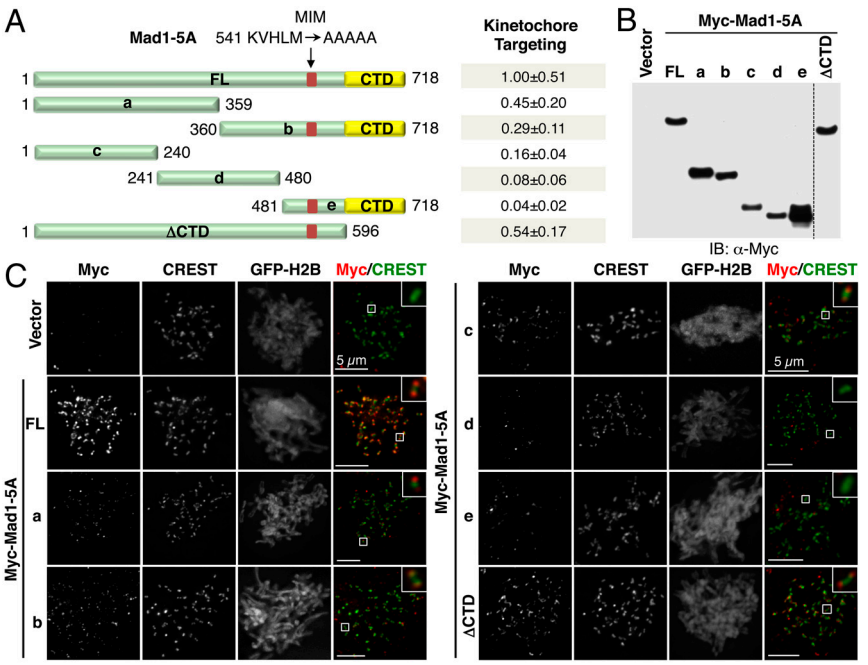

Fig. 2. Nonoverlapping Mad1 fragments exhibit detectable kinetochore binding. (*A*) Schematic drawing of Mad1 fragments used in this study. MIM, Mad2-interacting motif. The full-length Mad1 and fragments **b**, **e**, and ΔCTD had their MIM mutated to five alanines (5A). The relative intensity of the kinetochore signals of these Mad1 mutants was summarized on the right. The mean and standard deviation of Mad1 kinetochore signals from 10 cells for each construct were shown. (*B*) Lysates of HeLa Tet-On cells transfected with plasmids encoding various Mad1 fragments were blotted with anti-Myc. (*C*) Mitotic HeLa Tet-On cells transiently transfected with the indicated Mad1 fragments were stained with antibodies against Myc (red in the overlay) and CREST (green). GFP-H2B was cotransfected with Myc-Mad1 and used as a marker for transfected cells. (Scale bars, 5 μm).

None of the Mad1 fragments retained full kinetochore-targeting function (Fig. 2). Mad1-ΔCTD had about 50% of the kinetochore-binding activity of the full-length Mad1. Additional Mad1 fragments, **a**, **b**, and **c** exhibited weak, but detectable, kinetochore localization. Therefore, Mad1 has an extensive kinetochore-binding interface. The fact that nonoverlapping Mad1 fragments (**a**/**c** and **b**) retain residual kinetochore-targeting activity further suggests that Mad1 has multiple quasi-independent kinetochore-binding domains.

Because Mad1-ΔCTD dimerized with the endogenous Mad1 (Fig. S2*C*), the kinetochore signal of Mad1-ΔCTD could conceivably belong to this mixed dimer. The kinetochore signal of Myc-Mad1-ΔCTD was, however, still observed in cells depleted of the endogenous Mad1 by RNAi (Fig. S3), ruling out this possibility. Mad1 fragments **a**, **b**, and **c** did not dimerize with the endogenous Mad1. The residual kinetochore localization could not be caused by dimerization between the endogenous Mad1 and these fragments.

To confirm the involvement of the CTD in the kinetochore targeting of human Mad1, we next stably transfected GFP-Mad1 or GFP-Mad1-ΔCTD plasmids into HeLa cells and monitored the localization of the GFP-Mad1 fusion proteins using live-cell imaging (Fig. 3 *A* and *B*). When cells entered mitosis, Mad1 localized to unattached kinetochores (Fig. 3*A*). As mitosis progressed, the number of Mad1-positive kinetochore decreased. At metaphase, all kinetochores became attached to spindle microtubules and lacked Mad1 signals. By contrast, GFP-Mad1-ΔCTD failed to localize to kinetochores during any stages of mitosis (Fig. 3*B*). Both GFP-Mad1 and GFP-Mad1-ΔCTD were expressed at similar levels (Fig. 3*C*). Importantly, GFP-Mad1-ΔCTD retained the ability to localize to nuclear pores in interphase, ruling out global unfolding of GFP-Mad1-ΔCTD (Fig. 3*D*). These results validate a role of the CTD in the kinetochore targeting of Mad1 during unperturbed mitosis of human cells.

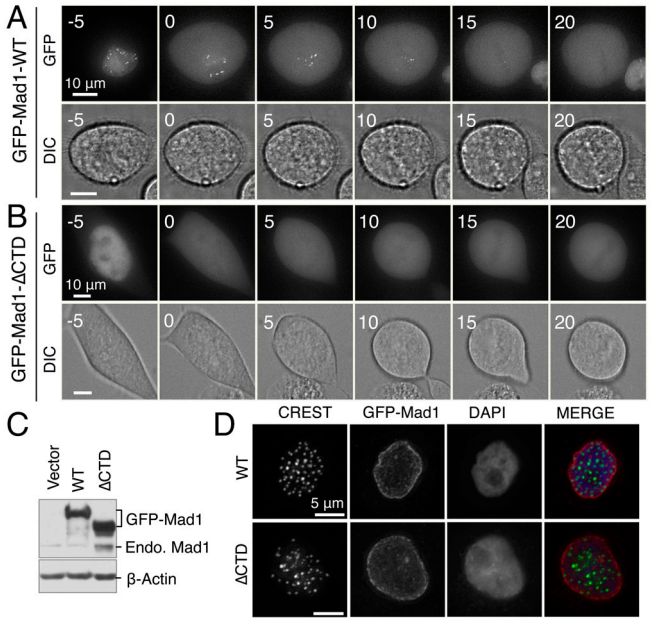

Fig. 3. The CTD is required for the kinetochore targeting of Mad1 during unperturbed mitosis in human cells. (*A* and *B*) HeLa Tet-On cells stably expressing GFP-tagged wild-type Mad1 (WT) (*A*) or the ΔCTD mutant (*B*) were analyzed using live-cell imaging. GFP and DIC images of a representative cell at the indicated times (in minutes) were shown. Nuclear envelope break down (NEBD) was set as time 0. (Scale bars, 10 μm). (*C*) Lysates of HeLa cells transfected with the empty vector and cells in (*A*) and (*B*) were blotted with anti-Mad1. The positions of GFP-Mad1 or the endogenous (Endo.) Mad1 proteins were indicated. Actin was used as the loading control. (*D*) Interphase HeLa cells stably expressing GFP-Mad1-WT or ΔCTD were stained with anti-GFP (pseudocolored red in merge), CREST (green), and DAPI (blue). (Scale bars, 5 μm).

It was surprising that Myc-Mad1-ΔCTD retained partial kinetochore targeting in fixed cells while GFP-Mad1-ΔCTD was undetectable by live-cell imaging. A possible explanation was that indirect immunofluorescence on fixed cells was more sensitive than live-cell imaging in detecting the kinetochore localization of Mad1. Consistent with this notion, GFP-Mad1-ΔCTD were indeed detectable at kinetochores in fixed cells (Fig. S4). Similar to Myc-Mad1-ΔCTD, the intensity of the GFP-Mad1-ΔCTD kinetochore signal was about 50% of that of GFP-Mad1-WT.

Identification of Two Classes of Mad1 CTD Mutants Deficient in Kinetochore Targeting. To further identify residues within Mad1 CTD critical for kinetochore binding, we performed structure-based mutagenesis and mutated conserved residues that had any exposed surface areas. Some of these residues targeted by mutagenesis were mostly buried. We introduced the Mad1 CTD mutations into full-length GFP-Mad1-5A and performed live-cell imaging experiments to examine their kinetochore localization (Fig. 4, Fig. S5).

Because T680 had been identified as a Plk1 phosphorylation site in vitro and had been implicated in Mad1 kinetochore targeting (20), we also mutated T680 to alanine even though T680 was completely buried. Contrary to a published report (20), we observed that the Mad1 T680A mutant retained kinetochore localization. Thus, we did not further pursue a potential regulation of Mad1 kinetochore targeting by Plk1.

Several GFP-Mad1-5A proteins harboring mutations in the CTD indeed failed to localize to kinetochores (Fig. 4, Fig. S5). These mutations could be divided into two classes. Class I mutations, including F629A, Y655A, L677A, F682A, and L709A, affected mostly buried hydrophobic residues (Fig. 5 *A* and *B*). Among them, F629, Y655, and L709 were located at the dimer interface. Class II mutations, including R617A, K619A, and R630A, altered surface-exposed residues in the CTD stem (Fig. 5*A*).

Mutations of several conserved surface-exposed residues on αC in the globular head, such as E710, F712, R714, and T716, did not affect the kinetochore targeting of GFP-Mad1-5A (Fig. 4, Fig. S5*B*). The top face of the globular head of the CTD was thus unlikely a direct kinetochore-binding surface, as we had originally envisioned. We hypothesized that the class I mutations disrupted the structure integrity or dimerization of Mad1 CTD, indirectly diminishing kinetochore binding of Mad1.

To test this hypothesis, we cotranslated HA- or Myc-Mad1 CTD in vitro in the presence of ^{35}S-methionine and performed immunoprecipitation with anti-HA beads. The wild-type HA-Mad1 CTD efficiently pulled down Myc-Mad1 CTD, confirming that the CTD indeed formed dimers in solution (Fig. 5*C*). The Myc-Mad1 CTD bands were more intense than the HA-Mad1 CTD bands, because the former contained six copies of the Myc tag and each Myc tag had a methionine. The HA-Mad1 CTD F629A, Y655A, L677A, F682A, and L709A mutants failed to bind to their Myc-tagged counterparts, indicating that these mutants did not form dimers. Among them, HA-Mad1 CTD F629A and L709A were not efficiently translated or pulled down with the anti-HA beads, suggesting that these mutations were more detrimental to the structural integrity of the Mad1 CTD monomer. Therefore, the class I mutations compromise kinetochore targeting of Mad1 by disrupting the dimerization of Mad1 CTD or its structural integrity or both. We note that Mad1-ΔCTD interacts with the endogenous Mad1 (Fig. S2*C*), suggesting that the N-terminal coiled coil domain of Mad1 was sufficient to maintain dimerization of the full-length Mad1. In the context of full-length Mad1, the CTD mutations are expected to cause local unfolding or splaying of the C-terminal end of Mad1.

In contrast to the class I mutants, the HA-tagged class II mutants (R617A, K619A, and R630A) efficiently pulled down their Myc-tagged counterparts (Fig. 5*C*), indicating that these mutants retained their ability to form dimers. Mutations of these residues reduced kinetochore targeting of Mad1, consistent with them

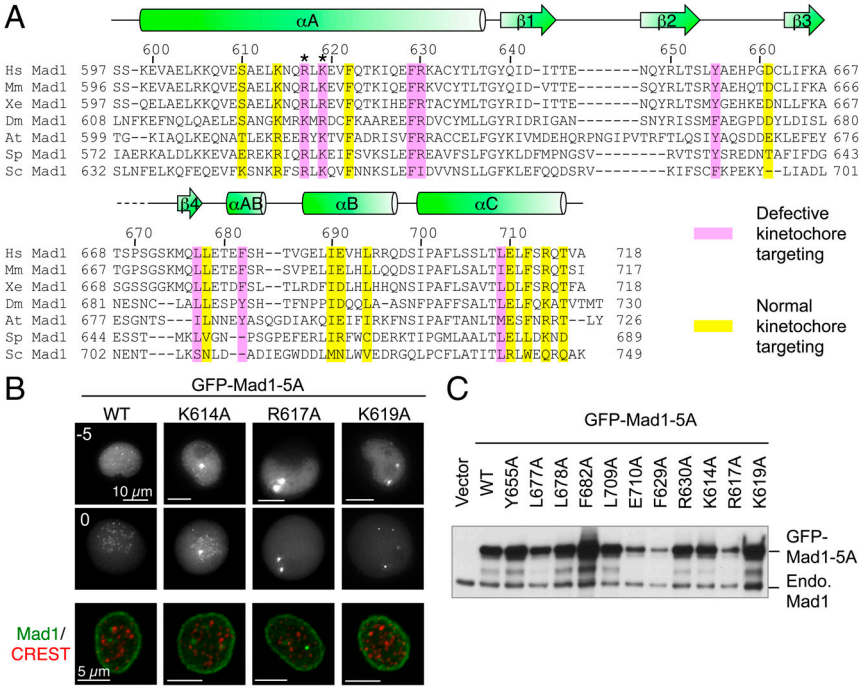

Fig. 4. Structure-based mutagenesis identifies Mad1 CTD residues critical for kinetochore targeting. (*A*) Sequence alignment of Mad1 CTD from different species with the secondary structural elements shown above. Residues whose mutations did or did not disrupt Mad1 kinetochore targeting were colored purple or yellow, respectively. R617 and K619 in the conserved RLK motif are labeled with asterisks. (*B*) HeLa Tet-On cells expressing the indicated GFP-Mad1-5A mutants were analyzed by live-cell imaging. GFP images of representative cells at NEBD (time 0) and at 5 min before NEBD were shown. Note that a fraction of the overexpressed GFP-Mad1-5A mutant proteins presumably aggregated and formed large foci that were not kinetochores. (Scale bars, 10 μm). The bottom box showed interphase cells expressing the same Myc-Mad1 mutants stained with anti-Myc (green) and CREST (red). (Scale bars, 5 μm). (*C*) Lysates of cells expressing GFP-Mad1-5A and mutants were blotted with anti-Mad1. The positions of GFP-Mad1-5A and the endogenous (Endo.) Mad1 proteins were labeled.

being directly involved in kinetochore binding. R617, K619, and R630 are located at the stem, suggesting that the stem of Mad1 CTD is a direct binding site of the kinetochore receptor of Mad1.

Bub1 Is Required for the Proper Kinetochore Targeting of Mad1. There are two class II residues, R617 and K619, residing in a conserved RLK motif (Fig. 4*A*). In yeast, Mad1 forms a complex with Bub1-Bub3 in nocodazole-arrested mitotic cells, but not in interphase cells (21). Interestingly, the RLK motif in yeast Mad1 is required for the checkpoint-stimulated binding between Mad1 and Bub1-Bub3. Cells harboring a Mad1 mutant with this motif mutated are

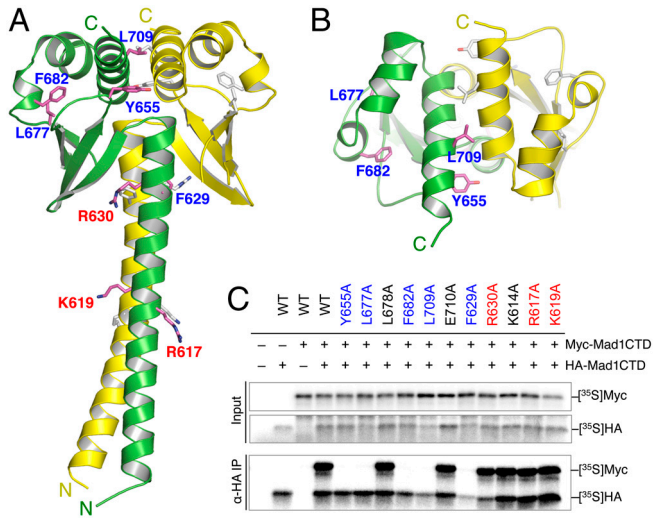

Fig. 5. Mutations of a conserved RLK motif in Mad1 CTD diminish kinetochore targeting of Mad1 without disrupting CTD dimerization. (*A* and *B*) Ribbon drawings of Mad1 CTD (*A*, side view; *B*, top view) with residues critical for kinetochore targeting in one monomer shown as purple sticks and labeled. The class I and II residues whose mutations did or did not disrupt dimerization were labeled with blue and red letters, respectively. The corresponding residues in the other monomer were shown in gray sticks and not labeled for clarity. (*C*) In vitro dimerization assays of Mad1 CTD mutants. HA- and Myc-tagged Mad1 CTD proteins were cotranslated in vitro in the presence of ^{35}S-methionine. The input (top box) and anti-HA IP (bottom box) were separated by SDS-PAGE and analyzed with a phosphor imager.

deficient in the spindle checkpoint. The biochemical functions of the Mad1-Bub1-Bub3 interaction are unclear, however. Our results now reveal a requirement of the conserved RLK motif of Mad1 in kinetochore targeting, suggest an underlying basis for the checkpoint defect caused by the mutation of this motif in yeast, and further implicate Bub1 or its associated proteins as conserved kinetochore receptors of Mad1.

There had been conflicting reports in the literature on the requirement of Bub1 in the kinetochore targeting of Mad1 in human cells (28, 29). We therefore examined whether Bub1 was required for Mad1 kinetochore localization during unperturbed mitosis of human cells, using live-cell imaging. In cells transfected with the control siRNA, GFP-Mad1-5A localized normally to kinetochores during mitosis (Fig. S6*A*). Depletion of Bub1 by RNAi greatly reduced the kinetochore localization of GFP-Mad1-5A. Depletion of Bub1 also diminished the kinetochore localization of the endogenous Mad1 in fixed HeLa cells (Fig. S6*B*). Despite the near complete depletion of Bub1 (Fig. S6*C*), the intensity of Mad1 staining at the kinetochore was only reduced to about 50% of that in control cells (Fig. S6*D*). The reduction of Mad1 staining at the kinetochores was not observed in cells stably expressing RNAi-resistant mCherry-Bub1 (Fig. S7), indicating that the observed effect of Bub1 RNAi was Bub1-dependent. Thus, Bub1 is required for proper kinetochore targeting of Mad1 in human cells, but it is not the sole kinetochore receptor of Mad1.

If Bub1 targeted Mad1 to kinetochores through an interaction with the RLK motif in the CTD, Bub1 depletion should not further reduce the already weakened kinetochore localization of the RLK-motif mutants. Indeed, depletion of Bub1 significantly reduced the kinetochore localization of Myc-Mad1, but not that of Myc-Mad1 R617A (Fig. 6). This result placed Bub1 and Mad1 CTD in the same pathway for targeting Mad1 to kinetochores, and strongly implicated Bub1 as a kinetochore receptor for the CTD.

Discussion

The unexpected structural similarity between the CTD of Mad1 and the kinetochore-binding CTDs of Spc25 and Csm1 has led us to identify a role of Mad1 CTD in kinetochore targeting. The Mis12 complex is the kinetochore receptor of the Spc25-Spc24 dimer (27, 30). Csm1 interacts with both the Mis12 complex and CENP-C. The lack of apparent sequence similarity between

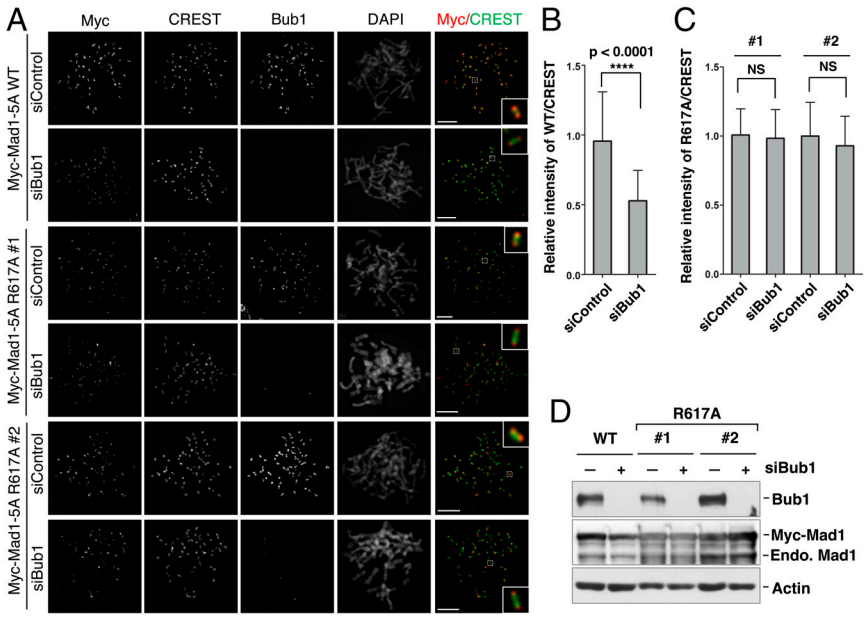

Fig. 6. Bub1 inactivation does not further reduce the residual kinetochore localization of the Mad1 RLK-motif mutant, R617A. (*A*) HeLa Tet-On cells stably expressing Myc-Mad1-5A WT or R617A (two independent clones, #1 and #2) were transfected with siControl or siBub1. Mitotic cells were stained with antibodies against Myc (red in the overlay), Bub1, CREST (green), and DAPI. (Scale bars, 5 μm). (*B* and *C*) Normalized kinetochore intensities of Myc-Mad1-5A WT (*B*) or R617A (*C*) of cells in (*A*). The mean and standard deviation of two independent experiments were shown. NS, not significant. (*D*) Lysates of cells in (*A*) were blotted with antibodies against Bub1, Mad1 and actin (used as a loading control). The positions of the Myc-tagged and endogenous (Endo.) Mad1 proteins were labeled.

the CTD of Mad1 and those of Spc25 and Csm1, however, suggests that they may not share the same kinetochore receptor. Furthermore, depletion of Ndc80 in human cells diminishes Mad1 kinetochore localization without affecting the kinetochore localization of the Mis12 complex (7, 31). The Mis12 complex is thus unlikely the direct kinetochore receptor of Mad1 CTD.

In yeast, Mad1 forms a mitosis-specific interaction with the Bub1-Bub3 complex (21). This interaction requires an RLK motif within Mad1 CTD. Cells harboring a Mad1 mutant with its RLK motif mutated are checkpoint deficient. Strikingly, we have shown here that the same RLK motif in the CTD is required for proper kinetochore targeting of Mad1 in human cells. Furthermore, depletion of Bub1 reduces the kinetochore localization of human Mad1. More importantly, Bub1 depletion does not further reduce the kinetochore localization of the Mad1 R617A mutant, suggesting that Bub1 and the RLK motif of Mad1 act in the same pathway to target Mad1 to kinetochores. These results strongly implicate Bub1 as a conserved kinetochore receptor for Mad1 CTD.

Unfortunately, despite extensive efforts and contrary to a previous report (32), we have failed to detect a physical interaction between human Mad1 and Bub1 either in cells or in vitro. Several nonoverlapping Mad1 fragments retain residual kinetochore targeting, indicating that Mad1 has an extensive kinetochore-binding surface with multiple quasi-independent contacting points. Consistently, depletion of Bub1 does not abolish Mad1 kinetochore localization. We propose that Mad1 forms contacts with multiple kinetochore proteins, one of which involves an interaction between Bub1 and Mad1 CTD, either directly or indirectly (Fig. 7). Because the Mad1 **e** fragment containing the CTD is insufficient for kinetochore binding, the interaction between Mad1 CTD and human Bub1 on its own might be too weak to be detected.

In yeast, a C-terminal fragment of Mad1 is sufficient for kinetochore localization and checkpoint signaling (18). Binding between yeast Mad1 CTD and Bub1-Bub3 thus makes a more substantial energetic contribution to the Mad1 kinetochore localization and hence might have higher affinity, allowing its detection. Another nonexclusive possibility is that Bub1 as a part of a larger kinetochore complex serves as the receptor for Mad1. The integrity of the Bub1-containing complex might be preserved in yeast cell lysates, but not in human cell lysates, explaining why the Bub1-Mad1 interaction is only observed in yeast.

The kinetochore binding of several checkpoint proteins, such as Bub1, BubR1, and Mps1, can be attributed to small, defined domains (33–35). By contrast, Mad1 uses an extensive, multivalent binding surface to interact with kinetochores. This mode of kinetochore targeting by Mad1 is unusual and has important implications for checkpoint signaling. In particular, this mechanism rationalizes the graded targeting of Mad1 to kinetochores under different conditions that activate the checkpoint. For example, the concentration of Mad1 at attached but untense kinetochores in Taxol-arrested mitotic human cells is much lower than that at unattached kinetochores in nocodazole-treated cells. Yet, the mitotic arrest of Taxol-treated cells is still dependent on Mad1-Mad2, suggesting that a small amount of Mad1 at the kinetochores is sufficient to sustain the checkpoint. A similar situation exists in cells depleted of the Ndc80 complex (7).

It is unclear whether the checkpoint-competent, reduced Mad1 kinetochore targeting under these conditions is caused by a distributive, uniform decrease of binding energy across the entire kinetochore-binding interface of Mad1 or by the selective disruption of a subset of discrete interactions between Mad1 and its kinetochore receptors. The current study has laid the foundation and provided the necessary tools for future experiments that will differentiate these two possibilities and establish how Mad1 integrates upstream checkpoint signals.

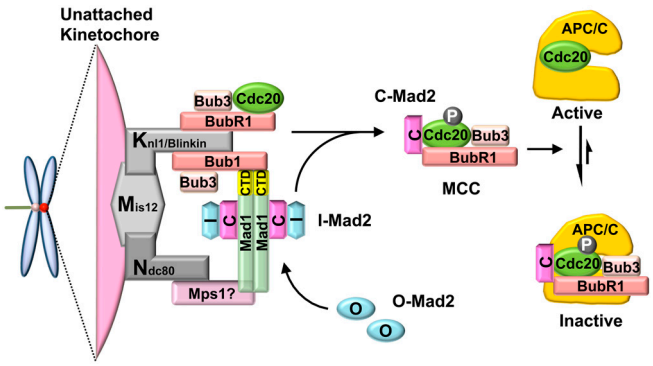

Fig. 7. A multivalency model for Mad1 kinetochore targeting. In this model, Mad1 is targeted to kinetochores through multiple quasi-independent contact sites with kinetochore receptors. One such contact site is between Bub1 and Mad1 CTD. Bub1-Bub3, BubR1-Bub3, and Mps1 are recruited to kinetochores by the KMN (Knl1/Blinkin-Mis12-Ndc80) network of proteins. Ndc80 and Mps1 are required for proper Mad1 kinetochore targeting. It remains to be established whether the N-terminal region of Mad1 directly contacts Ndc80 or Mps1. At the kinetochores, the Mad1-Mad2 core complex promotes the conformational activation of Mad2, Mad2 binding to Cdc20, and APC/C inhibition.

Materials and Methods

Protein Purification, Crystallization, and Structure Determination. Recombinant human Mad1$^{597–718}$ was expressed in bacteria and purified with a combination of affinity and conventional chromatography. The seleno-methionine labeled Mad1$^{597–718}$ was produced using the methionine biosynthesis inhibition method (36). Mad1$^{597–718}$ was crystallized at 20 °C using the hanging-drop vapor-diffusion method with a reservoir solution containing 0.1 M sodium cacodylate (pH 6.2), 26% (wt/vol) PEG 1500 and 1 mM reduced L-glutathione. All diffraction data were collected at the Advanced Photon Source and processed with HKL3000 (37). Phases were obtained from a selenium-SAD experiment. Phenix was used to identify the selenium sites, calculate density-modified experimental maps, and build the initial model (38). Additional model building and refinement were performed with COOT (39) and Phenix. MolProbity was used for structure validation and indicated that all residues were in the Ramachandran favored/allowed regions (40). Data collection and structure refinement statistics are summarized in Table S1. Details are included in *SI Text*.

Cell Culture and Transfection. HeLa Tet-On (Clontech) cells were grown in Dulbecco's modified Eagle's medium (DMEM; Invitrogen) supplemented with 10% fetal bovine serum (FBS). Plasmid and siRNA transfections were performed with the Effectene reagent (Qiagen) and Lipofectamine RNAiMAX (Invitrogen), respectively. Details are included in *SI Text*.

Live-Cell Imaging. Cells were grown and transfected in 6-well plates. At 20–24 h after transfection, cells were passaged onto chambered coverslips (LabTek), incubated with 2 mM thymidine (Sigma) for 14–16 h, and released into fresh media for 4–6 h prior to taking images. Differential interference contrast (DIC) and GFP fluorescence images were obtained at 5-min intervals with a DeltaVision deconvolution fluorescence microscope (Applied Precision). Details are included in *SI Text*.

Immunofluorescence, Immunoprecipitation, and Immunoblotting. For interphase Mad1 localization, HeLa Tet-On cells were directly grown in 4-well chambered slides (LabTek) and stained with the appropriate antibodies. For mitotic Mad1 localization, cells were grown in 6-well plates and incubated with 500 nM nocodazole (Sigma) for 16–18 h. Mitotic cells were harvested by shake-off, resuspended in hypotonic solution (55 mM KCl), spun onto slides with Shandon Cytospin 4 (Thermo Fisher), and stained with the appropriate antibodies. Details of staining procedure, image acquisition, and quantification are included in *SI Text*. Standard procedures were used for immunoprecipitation and immunoblotting. Details are included in *SI Text*.

In Vitro Binding Assay. To assay Mad1-CTD dimerization, same amounts of plasmids encoding Myc- or HA-tagged Mad1-CTD WT or point mutants were translated in reticulocyte lysate in the presence of ^{35}S-methionine. Affi-Prep protein A beads (Bio-Rad) covalently coupled to α-HA monoclonal antibodies (Roche) were incubated with ^{35}S-labeled Mad1-CTD, and washed three times with Tris-buffered saline (TBS) containing 0.05% Tween. The bound proteins were separated by SDS-PAGE and analyzed with a phosphor imager (Fujifilm).

Note. A recent study by Schmitzberger and Harrison (EMBO Reports, 13, 216-222, 2012) shows that the centromere proteins CENP-O and CENP-P also contain RWD domains, suggesting that this domain might be a common module for kinetochore architecture.

ACKNOWLEDGMENTS. We thank Andrea Musacchio and Marina Mapelli for the Mad1 CTD expression plasmid and for sharing results prior to publication. We also thank Maojun Yang for assistance with X-ray diffraction data collection. This research was supported by grants from the National Institutes of Health (GM085004 to X.L.) and the Welch Foundation (I-1441 to H.Y.). S.K. is the recipient of a training grant from the Cancer Prevention and Research Institute of Texas (CPRIT). H.Y. is an Investigator with the Howard Hughes Medical Institute. Results shown in this report are derived from work performed at Argonne National Laboratory, Structural Biology Center at the Advanced Photon Source. Argonne is operated by UChicago Argonne, LLC, for the Department of Energy, Office of Biological and Environmental Research under contract DE-AC02-06CH11357.

1. Bharadwaj R, Yu H (2004) The spindle checkpoint, aneuploidy, and cancer. *Oncogene* 23:2016–2027.
2. Qi W, Yu H (2006) The spindle checkpoint and chromosomal stability. *Genome Dynamics* 1:116–130.
3. Musacchio A, Salmon ED (2007) The spindle-assembly checkpoint in space and time. *Nat Rev Mol Cell Biol* 8:379–393.
4. Yu H (2002) Regulation of APC-Cdc20 by the spindle checkpoint. *Curr Opin Cell Biol* 14:706–714.
5. Yu H (2007) Cdc20: a WD40 activator for a cell cycle degradation machine. *Mol Cell* 27:3–16.
6. Peters JM (2006) The anaphase promoting complex/cyclosome: a machine designed to destroy. *Nat Rev Mol Cell Biol* 7:644–656.
7. Martin-Lluesma S, Stucke VM, Nigg EA (2002) Role of Hec1 in spindle checkpoint signaling and kinetochore recruitment of Mad1/Mad2. *Science* 297:2267–2270.
8. Bharadwaj R, Qi W, Yu H (2004) Identification of two novel components of the human NDC80 kinetochore complex. *J Biol Chem* 279:13076–13085.
9. Luo X, Tang Z, Rizo J, Yu H (2002) The Mad2 spindle checkpoint protein undergoes similar major conformational changes upon binding to either Mad1 or Cdc20. *Mol Cell* 9:59–71.
10. Luo X, et al. (2004) The Mad2 spindle checkpoint protein has two distinct natively folded states. *Nat Struct Mol Biol* 11:338–345.
11. Sironi L, et al. (2002) Crystal structure of the tetrameric Mad1-Mad2 core complex: implications of a 'safety belt' binding mechanism for the spindle checkpoint. *EMBO J* 21:2496–2506.
12. Mapelli M, Massimiliano L, Santaguida S, Musacchio A (2007) The Mad2 conformational dimer: structure and implications for the spindle assembly checkpoint. *Cell* 131:730–743.
13. Yang M, et al. (2008) Insights into mad2 regulation in the spindle checkpoint revealed by the crystal structure of the symmetric mad2 dimer. *PLoS Biol* 6:e50.
14. De Antoni A, et al. (2005) The Mad1/Mad2 complex as a template for Mad2 activation in the spindle assembly checkpoint. *Curr Biol* 15:214–225.
15. Luo X, Yu H (2008) Protein metamorphosis: the two-state behavior of Mad2. *Structure* 16:1616–1625.
16. Mapelli M, Musacchio A (2007) MAD contortions: conformational dimerization boosts spindle checkpoint signaling. *Curr Opin Struct Biol* 17:716–725.
17. Kulukian A, Han JS, Cleveland DW (2009) Unattached kinetochores catalyze production of an anaphase inhibitor that requires a Mad2 template to prime Cdc20 for BubR1 binding. *Dev Cell* 16:105–117.
18. Kastenmayer JP, Lee MS, Hong AL, Spencer FA, Basrai MA (2005) The C-terminal half of *Saccharomyces cerevisiae* Mad1p mediates spindle checkpoint function, chromosome transmission fidelity and CEN association. *Genetics* 170:509–517.
19. Chung E, Chen RH (2002) Spindle checkpoint requires Mad1-bound and Mad1-free Mad2. *Mol Biol Cell* 13:1501–1511.
20. Chi YH, et al. (2008) Requirements for protein phosphorylation and the kinase activity of polo-like kinase 1 (Plk1) for the kinetochore function of mitotic arrest deficiency protein 1 (Mad1). *J Biol Chem* 283:35834–35844.
21. Brady DM, Hardwick KG (2000) Complex formation between Mad1p, Bub1p and Bub3p is crucial for spindle checkpoint function. *Curr Biol* 10:675–678.
22. Wei RR, et al. (2006) Structure of a central component of the yeast kinetochore: the Spc24p/Spc25p globular domain. *Structure* 14:1003–1009.
23. Ciferri C, et al. (2008) Implications for kinetochore-microtubule attachment from the structure of an engineered Ndc80 complex. *Cell* 133:427–439.
24. Corbett KD, et al. (2010) The monopolin complex crosslinks kinetochore components to regulate chromosome-microtubule attachments. *Cell* 142:556–567.
25. Nameki N, et al. (2004) Solution structure of the RWD domain of the mouse GCN2 protein. *Protein Sci* 13:2089–2100.
26. Burroughs AM, Jaffee M, Iyer LM, Aravind L (2008) Anatomy of the E2 ligase fold: implications for enzymology and evolution of ubiquitin/Ub-like protein conjugation. *J Struct Biol* 162:205–218.
27. Petrovic A, et al. (2010) The MIS12 complex is a protein interaction hub for outer kinetochore assembly. *J Cell Biol* 190:835–852.
28. Klebig C, Korinth D, Meraldi P (2009) Bub1 regulates chromosome segregation in a kinetochore-independent manner. *J Cell Biol* 185:841–858.
29. Liu ST, Rattner JB, Jablonski SA, Yen TJ (2006) Mapping the assembly pathways that specify formation of the trilaminar kinetochore plates in human cells. *J Cell Biol* 175:41–53.
30. Cheeseman IM, Chappie JS, Wilson-Kubalek EM, Desai A (2006) The conserved KMN network constitutes the core microtubule-binding site of the kinetochore. *Cell* 127:983–997.
31. Kline SL, Cheeseman IM, Hori T, Fukagawa T, Desai A (2006) The human Mis12 complex is required for kinetochore assembly and proper chromosome segregation. *J Cell Biol* 173:9–17.
32. Seeley TW, Wang L, Zhen JY (1999) Phosphorylation of human MAD1 by the BUB1 kinase in vitro. *Biochem Biophys Res Commun* 257:589–595.
33. Taylor SS, McKeon F (1997) Kinetochore localization of murine Bub1 is required for normal mitotic timing and checkpoint response to spindle damage. *Cell* 89:727–735.
34. Kiyomitsu T, Obuse C, Yanagida M (2007) Human Blinkin/AF15q14 is required for chromosome alignment and the mitotic checkpoint through direct interaction with Bub1 and BubR1. *Dev Cell* 13:663–676.
35. Stucke VM, Baumann C, Nigg EA (2004) Kinetochore localization and microtubule interaction of the human spindle checkpoint kinase Mps1. *Chromosoma* 113:1–15.
36. Van Duyne GD, Standaert RF, Karplus PA, Schreiber SL, Clardy J (1993) Atomic structures of the human immunophilin FKBP-12 complexes with FK506 and rapamycin. *J Mol Biol* 229:105–124.
37. Otwinowski Z, Minor W (1997) Processing X-ray diffraction data collected in oscillation mode. *Methods Enzymol* 276:307–326.
38. Adams PD, et al. (2010) PHENIX: a comprehensive Python-based system for macromolecular structure solution. *Acta Crystallogr D* 66:213–221.
39. Emsley P, Cowtan K (2004) COOT: model-building tools for molecular graphics. *Acta Crystallogr D* 60:2126–2132.
40. Chen VB, et al. (2010) MolProbity: all-atom structure validation for macromolecular crystallography. *Acta Crystallogr D* 66:12–21.